



An eddy-borne Argo float measurement experiment in the South China Sea

Chunyong Ma^{1,2} · Zhanwen Gao¹ · Siqing Li¹ · Shuo Li¹ · Ge Chen^{1,2}

Received: 6 June 2019 / Accepted: 18 August 2020 / Published online: 25 August 2020
© Springer-Verlag GmbH Germany, part of Springer Nature 2020

Abstract

Argo floats can be used to collect unique and spatiotemporally continuous eddy profiles as they are carried forward within eddies. Using satellite altimeter data, we designed and conducted an eddy-borne Argo float measurement experiment in a South China Sea (SCS) eddy generated in the southwest region of Taiwan. The Argo float was deployed at a location that was estimated to be in the eddy corridor on December 31, 2016. As a result, the Argo float continuously observed the target eddy for more than 2 months, and successfully obtained 62 valuable daily temperature (T) and salinity (S) profiles inside this eddy. From this Argo float's movement, the smooth transition of the float speed and heading revealed that the eddy splitting identified by satellite altimeter data should be an artifact from January 14 to 18, 2017. In addition, it is found that the depth of thermocline is negative correlated with the normalized radial distance of the float to the eddy center, and the bowl-like shape of the thermocline depth can be revealed. The T-S diagram of Argo float profiles indicated that eddy water should be derived from the Kuroshio Current. The design and implementation of this experiment are a successful example of SCS eddy observation, which will undoubtedly guide oceanographers to obtain more effective eddy data. The development of an “Eddy-Argo” program designed for eddy observation is worthy of additional research in the future.

Keywords South China Sea (SCS) eddies · Argo floats · Satellite altimeter · Tracking measurements

1 Introduction

Eddies have been detected globally with the development of ocean satellite altimeter measurements, and their distribution has been widely studied (e.g., Chelton et al. 2007, 2011). The surface signatures and lifespan of South China Sea (SCS) eddies have also been well investigated based on the merged data products of satellite altimeters (Wang et al. 2003; Yuan et al. 2007; Xiu et al. 2010; Chen et al. 2011). To broadly study the subsurface SCS eddy structure, scientists have collected numerous in situ eddy measurements from cruise surveys (Wade and Heywood 2001; Hu et al. 2011; Nan et al.

2011; Chen et al. 2012; Chu et al. 2014; He et al. 2018) and have employed some unmanned observation platforms, which usually include moorings (Wang et al. 2015; Chen et al. 2015; Zhong et al. 2017), gliders (Zaba and Rudnick 2016; Shu et al. 2016, 2018) and Argo floats (Zhang et al. 2014; Dong et al. 2014).

Based on in situ SCS eddy data, northern SCS eddies have been widely studied (e.g., Chen et al. 2012; Nan et al. 2015). Chen et al. (2010) used Argo and sea level anomaly (SLA) data from altimetry, in which the SLA is defined as the anomaly between the actual sea surface height and the mean sea surface height, to analyze the seasonal variability of the Luzon warm eddy. Hu et al. (2012) used cruise CTD and ADCP data observed in January 2010, in combination with satellite altimeter data and Argo float data, and the analysis results revealed a high-salinity water prism centered at 21° N, 118.5° E in the subsurface layer west of the Luzon Strait. They proposed that the eddy was generated by the nonlinearity of the Rossby waves from the North West Pacific. Zhang et al. (2013) used long-term moored observations to investigate a pair of meso-scale eddies that were generated southwest of Taiwan and found that both baroclinic and barotropic instabilities were important for the generation and growth of the eddy pair.

Responsible Editor: Aida Alvera-Azcárate

✉ Ge Chen
gechen@ouc.edu.cn

¹ College of Information Science and Engineering, Ocean University of China, 238 Songling Road, Qingdao, Shan Dong Province 266100, People's Republic of China

² Laboratory for Regional Oceanography and Numerical Modeling, Qingdao National Laboratory for Marine Science and Technology, No.1 WenHai Road, Qingdao 266200, People's Republic of China

Zhang et al. (2016) designed and conducted the South China Sea Mesoscale Eddy Experiment (S-MEE) in the northern SCS, and captured the full-depth 3D structure of an anticyclonic and cyclonic eddy pair. They suggested that the origin of the anticyclonic eddy was from the shedding of the Kuroshio Current. So far, the generation and propagation mechanism of the SCS eddies have not been fully studied, and more types of observation data in this region are needed.

In recent years, several Argo float-based eddy measurement experiments have been conducted. Xu et al. (2016) deployed 17 Argo floats and obtained over 3000 hydrographic profiles to observe the effect of mesoscale eddies on mode-water subduction and transport in the North Pacific. In the SCS, Zhang et al. (2015) selected 6 Argo floats inside an anticyclonic eddy and revealed two important dynamical processes (radial displacement and vertical fluctuations) of this eddy. However, the floats they used come from Coriolis Argo Global Data Assembly Centre and were not deployed by themselves. In contrast, this study aimed to design a novel eddy-borne Argo float measurement experiment deploying an Argo float in the northern SCS to obtain continuous tracking observation data. To find a strong SCS target eddy, satellite altimeter eddy identification and tracking algorithms have been used (Liu et al. 2016; Sun et al. 2017). SCS eddy propagation prediction and vertical “eddy center” (Li et al. 2017) determination algorithms were used to guide our choice of the Argo float deployment location and parking depth.

This paper is organized as follows: the data and methods used in this study are described in section 2 and 3, respectively. Section 4 introduces the implementation of this experiment. In section 5, we present the temporal evolution of the target eddy using SLA data. The temperature and salinity vertical profiles collected from both Argo floats are shown in this section. Section 6 describes the 3D structure of the eddy and discusses the source of the water trapped by the eddy. The key results are summarized in section 7.

2 Data

This experiment can be divided into three stages: (1) statistics of historical eddy parameters in the northeastern SCS; (2) deployment station position determination and Argo float deployment; and (3) eddy data collection and Argo float parameter remote adjustment. In the first stage, SCS eddy corridors and mean maximum temperature anomaly depth were extracted based on the historical data of satellite altimeter and Argo float respectively, which will be described in detail in section 2.1 and section 2.2 below. These statistical results provide important references for the target eddy selection and parking depth setting of the Argo float. In the second stage of Argo deployment, the target eddy and deployment station position were determined under the constraints of the planning route.

As there was no chance to directly put the Argo float into the target eddy, it was a challenge to find a suitable position outside the eddy by combining the estimated directions of sea current and eddy movement. In the third stage, after Argo float deployment, Argo float parameters could still be remotely adjusted based on in situ observations. As a result, the float was trapped by the eddy for 67 days and provided measurements of its vertical structure until February 24, 2017.

2.1 SCS SLA data

The daily gridded SLA data used in this study are delayed time products generated by Archiving, Validation, and Interpretation of Satellite Oceanographic (AVISO) (<http://www.aviso.oceanobs.com>) from a combination of multiple altimeter satellites (ERS-1/2, TOPEX/Poseidon, ENVISAT, and Jason-1/Jason-2). The spatial resolution of the dataset is $0.25^\circ \times 0.25^\circ$ and the experimental area range is $5\text{--}25^\circ \text{N}$ and $105\text{--}125^\circ \text{E}$.

SLA data were used throughout the three stages of this experiment. In the first stage, the SLA dataset from January 1999 to December 2015 were used to determine the eddy corridors in the SCS. In the second stage, SLA data were used to select the target eddy, and track the eddy from November 20 to December 12, 2016. After the Argo float deployment, SLA data from December 13, 2016, to February 24, 2017, were used to observe the intersection of the Argo float with the target eddy.

In addition, the SLA data can be used to calculate the dynamic surface parameters of the eddy. The geostrophic velocity of the eddy is computed from the SLA gradients (Liu et al. 2016):

$$u = -\frac{g}{f} \frac{\partial SLA}{\partial y} \quad (1)$$

$$v = \frac{g}{f} \frac{\partial SLA}{\partial x} \quad (2)$$

$$U = \sqrt{u^2 + v^2} \quad (3)$$

where g is the acceleration due to gravity; $f = 2\Omega \sin\varphi$ is the Coriolis parameter; and Ω is the rotation rate of the earth, with φ being the latitude. ∂x and ∂y are the eastward and northward distances, respectively. u and v are zonal and meridional geostrophic velocity, respectively and U is the velocity magnitude.

2.2 Argo float data

The Argo float deployed in this experiment was produced by the China National Ocean Technology Center (CNOTC), and the float could be remotely controlled through the Chinese Beidou satellite system, which provides short message

communication services. In this paper, this type of Argo float is called the “B-Argo.” The float parameters including the working cycle and parking depth could be remotely adjusted. Here, the working cycle represents the time needed for the Argo float to descent and ascent. The parking depth is defined as a position at which the Argo float is stabilized by making the float density equal to the ambient pressure.

In the first stage of this experiment, historical Argo float profiles were downloaded in the range of 18–24° N and 116–122° E from 1997 to 2016 through the Coriolis Argo Global Data Assembly Centre in France (<ftp://ftp.ifremer.fr/ifremer/argo/>). The climatological data we used in this study come from the latest climatological dataset named CSIRO Atlas of Regional Sea 2009 (CARS2009 <http://www.marine.csiro.au/dunn/cars2009/>), and its spatial resolution is 0.5° × 0.5°. All temperature anomaly (TA) profiles were obtained by removing the climatological temperature profile from the Argo float data.

The Argo profiles obtained inside the anticyclonic eddy boundary (SLA contour corresponding to the maximum geostrophic velocity) were used to compose the mean temperature anomaly profile representative of anticyclonic eddies in this region. As a result, a total of 244 historical TA profiles were selected, and the mean profile is plotted in Fig. 1a. It is found that the depth of the maximum TA (DMTA) was near 90 m. In the Argo float observation experiment of Xu et al. (2016), parking depth was selected which was closest to the DMTA of mean profile. Similarly, the parking depth of the B-Argo was also chosen the location closest to the DMTA and finally determined to be 150 m in our experiment. The reason for this choice was that B-Argo could only hover at a few fixed depths and 150 m was the closest parking depth to 90 m.

In the third stage of this experiment, we obtained 62 effective B-Argo profiles, and 5 profiles failed to be uploaded in 67 days (from December 20, 2016, to February 24, 2017) due to unstable communication. Considering the power and communication efficiency, this float only recorded and uploaded temperature and salinity measurements until 500 m depth. As

additional observational data, 10 profiles from the Argo float 2901480 within this target eddy obtained from March 5, 2017, to April 10, 2017, are analyzed. The temperature and salinity profiles until 1000 m depth provided by this float were all valid. Finally, a total of 72 profiles were collected (B-Argo: 62 profiles, Argo 2901480: 10 profiles) within the target eddy.

3 Method

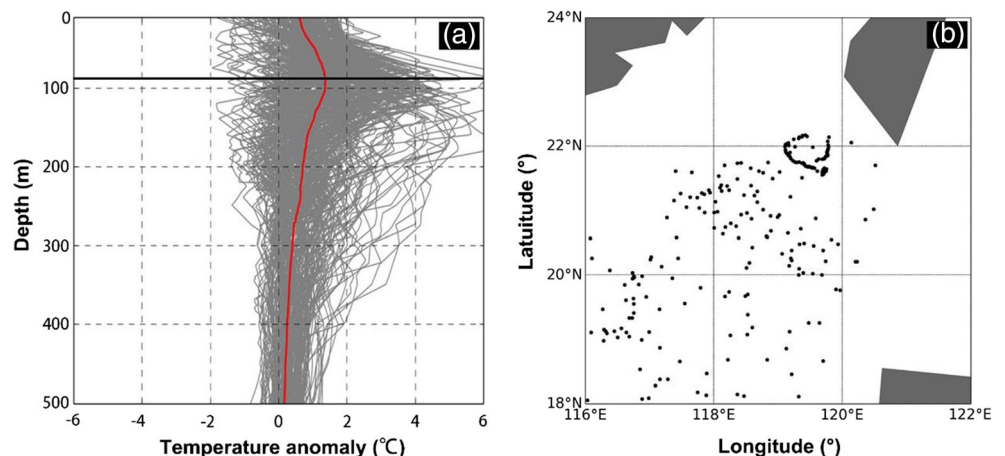
3.1 SLA-based eddy identification and tracking

SLA data derived from satellite altimeter sea surface height observations have been extensively used to identify and track mesoscale eddies (Chelton et al. 2011). The SLA-based eddy identification algorithm implemented by Liu et al. (2016) is used in this work. In order to determine the boundary of the cyclonic (anticyclonic) eddy, an SLA contour is searched from a minimum (maximum) value upward (downward) until 0 to see if it satisfies the following criteria:

- (1). contain no more than one “seed” (local maximum/minimum);
- (2). pixel count should be greater than 8 pixels and less than 1000 pixels;
- (3). pass a shape test with error less than 55%, where the error is defined as the ratio between the areal sum of closed SLA contour deviations from its equal area circle and the area of that circle
- (4). amplitude is greater than or equal to 2.0 cm. (amplitude is defined as the SLA difference between the seed and the SLA contour)

The outermost closed SLA contour (Liu et al. 2016) which satisfies the above conditions represents the eddy effective boundary (C_{eff}) and the “seed” of local maximum/minimum value represents the eddy center. In addition, criterion (4) is based on the fact that the accuracy of the AVISO gridded

Fig. 1 Argo float profiles and positions near the deployment station. **a** TA profiles located within anticyclonic eddies. The mean profile is indicated by the red line, and the horizontal black line indicates the location of the maximum TA. The locations of the historical Argo profiles we used are shown in **b**



altimeter data is about 2.0 cm (Dufau et al. 2016). The calculation formula of area-averaged vorticity (ζ) is as follows (Tian et al. 2020):

$$\zeta = \frac{1}{N} \sum_{i=1}^N \left(\frac{\partial v}{\partial x} - \frac{\partial u}{\partial y} \right) \quad (4)$$

where N is the number of gridded SLA data points located within the eddy boundary. ∂x , ∂y , ∂u , and ∂v are detailed described in section 2.1. The area-averaged vorticity value is the mean of local values at all grid points inside the eddy.

An eddy tracking algorithm (Sun et al. 2017) was adopted to track the eddies in the next day (t_2) based on the eddy identification results of day t_1 . Firstly, the next eddy will be searched within a specific range which was set to 50 km. Secondly, if more than one eddies (k) fall within the search range, the target eddy is then assigned as the one with minimum $S_{t_1,k}$, a dimensionless similarity parameter (Penven et al. 2005) computed for each of the k candidates and defined as:

$$S_{t_1,k} = \sqrt{\left(\frac{\Delta E}{E_0}\right)^2 + \left(\frac{\Delta d}{d_0}\right)^2 + \left(\frac{\Delta a}{a_0}\right)^2 + \left(\frac{\Delta A}{A_0}\right)^2} \quad (5)$$

where ΔE , Δd , Δa , and ΔA are respectively the variations of kinetic energy, distance, amplitude, and area between the eddy identified at time t_1 and the eddies identified within the search range at t_2 . The following characteristic values are used in our computation: $E_0 = 100 \text{ cm}^2/\text{s}^2$, $d_0 = 0.25^\circ$, $a_0 = 2 \text{ cm}$, and $A_0 = \pi 60^2 \text{ km}^2$ (Penven et al. 2005). As a result, the eddy which has the minimum $S_{t_1,k}$ will be determined as the continuous eddy in the next day (t_2). The tracking process is executed iteratively until all identified eddies are examined.

A total of 427 anticyclonic eddies and 495 cyclonic eddies trajectories were extracted. These trajectories had lifespans of more than 30 days in the SCS from January 1999 to December 2015, and the anticyclonic eddy trajectory data were used for the eddy corridor determination discussed in the next section.

3.2 SCS eddy corridor determination

There are 427 anticyclonic eddy trajectories in our SCS eddy dataset with lifespans greater than 30 days. To determine the main eddy corridors in the SCS, we apply the following procedure. First, eddy trajectories are partitioned into line segments based on the minimum description length (MDL) principle. Second, line segments are clustered using the DBSCAN (Density-Based Spatial Clustering of Applications with Noise) algorithm (Ester et al. 1996). There are two important parameters in this algorithm, (1) Eps, which represents the search radius of each line segment; and (2) Minpts, which represents the threshold of the number of line segments within the search radius. In this work, the Eps and Minpts values

are 50 km and 3, respectively, for the trajectories clustering of the eddies detected from altimetry. Third, the representative trajectory is determined to describe the overall movement of the eddies within the eddy corridor. Readers can refer to Lee et al. (2007) if they are interested in the clustering method.

As a result, five anticyclonic eddy corridors were extracted in the SCS, one of which contains 32.1% of all eddy tracks. As shown by the purple line in Fig. 2, this eddy corridor extends from the Luzon Strait to the southern tip of Hainan Island.

4 Implementation of an eddy-borne B-Argo profiling experiment

4.1 Target eddy observation and B-Argo deployment

Several days before deploying the B-Argo, we used the SLA data to identify mesoscale eddies in the SCS, and we found an anticyclonic eddy coming from the Luzon Strait. The eddy was tracked for 23 days from November 20 to December 12, 2016 (the trajectory is shown by a green line in Fig. 2). Its movement direction predominantly coincided with the eddy corridor. Therefore, the target eddy was expected to propagate southwestward following this path with a long lifespan.

The cruise was planned to start at Shanghai, pass through the Luzon Strait, and cross the Mariana Trench (indicated by the dashed red line in Fig. 2), but there was no intersection between the ship route and the target eddy (Fig. 3a); it was not possible to deploy the B-Argo float directly inside the eddy. From the forecast data of the National Marine Environmental Forecasting Center (NMEFC), the direction of the upper ocean currents in the target area was northeast. Meanwhile, the target eddy was moving westward. Therefore, considering the route constraints and the above movement directions, the yellow star in Fig. 2 was considered to be an appropriate deployment station. On December 13, 2016, we deployed the float at 20.4° N , 119.32° E , southwest of the target eddy, waiting for the arrival of the target eddy.

4.2 B-Argo parameters adjustment after deployment

To verify the movement direction of the B-Argo, we first set the cycle to 2 days firstly. From Fig. 3a and b, it can be determined that the B-Argo moved northwest by approximately 20 km per day, which was much faster than the eddy. Therefore, it was possible that the B-Argo could leave the corridor before the target eddy crossed its trajectory. Based on the eddy identification data from December 13 to 15, the eddy position and radius over the next 5 days were estimated using a linear extrapolation algorithm (Fig. 3b). The predicted position of the B-Argo could also be calculated using a similar algorithm based on its trajectory on December 13 and 15.

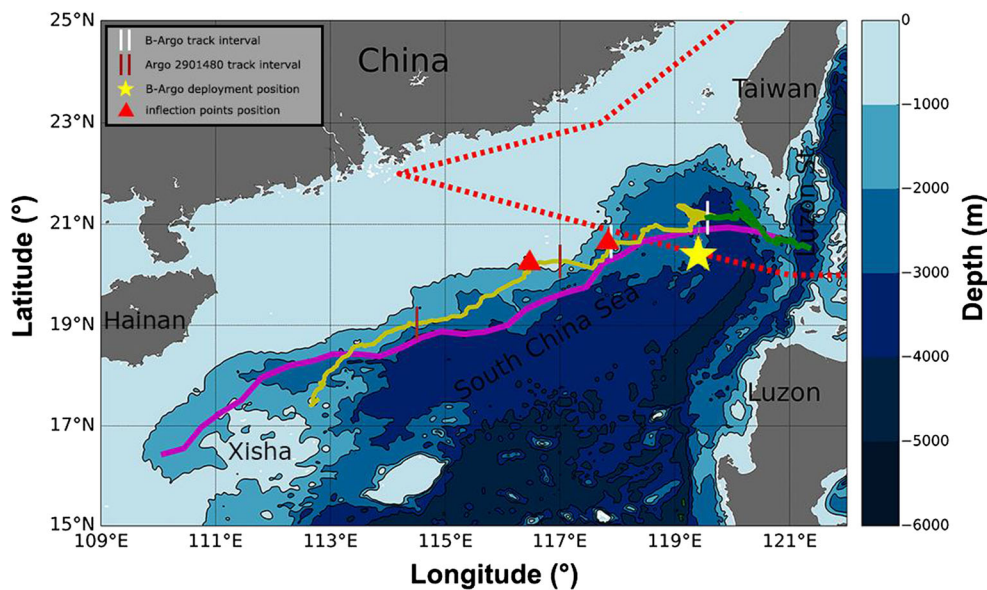


Fig. 2 The deployment strategy for the B-Argo float and eddy trajectory tracked using altimeter data. The color shading shows the bathymetry. The dashed red line denotes the planning route. The purple line indicates the eddy corridor in the northern region of the SCS. The green line is the trajectory of the target eddy detected from altimeter data from November 20 to December 12, 2016. The yellow line is the trajectory of the target eddy from December 13, 2016, to June 2, 2017. The two white vertical

lines represent the tracking interval of the B-Argo to the target eddy from December 20, 2016, to February 24, 2017. The two red vertical lines represent the tracking interval of the Argo float 2901480 to the target eddy from March 5, 2017, to April 10, 2017. The yellow star is the position where the B-Argo was deployed, and the red triangles are the locations of two inflection points during the target eddy movement

Comparing the predicted eddy and B-Argo positions after 3 days and 5 days, it was expected that the B-Argo would be trapped by the eddy 5 days after. Therefore, to avoid the B-Argo not being trapped by the eddy, we decided to park the Argo float at a depth of 1000 m for 5 days.

On December 20, the altimetry maps indicated that the Argo float was located within the eddy, as shown in Fig. 3c. To verify that the B-Argo was trapped by the eddy, we calculated the TA profile by removing the climatological profile of the region (CARS2009) from the temperature profile sampled by the B-Argo on December 20, 2016 (Fig. 3d). Here, B-Argo data were interpolated to the same depth intervals as the climatological profile using the single-value spline method. As shown in Fig. 3d, at a depth of 110 m, there was a clear warm anomaly, which confirmed that the B-Argo was trapped within the target eddy.

5 Eddy evolution

5.1 Daily evolution of the target eddy

From the trajectory obtained by the eddy identification and tracking method, it is found that the propagation directions and positions of the target eddy were similar to the eddies within the eddy corridor in the north SCS (Fig. 2). The eddy was detected for the first time at the south of Taiwan and propagated westward along the

1000 m isobath until reaching the vicinity of Xisha. The eddy lifecycle lasted 194 days, from November 20, 2016, to June 2, 2017. The westward propagation trajectory of the target eddy was roughly along the isoline at the depth of 1000 m, but it hardly crossed this isoline, especially in the shallow area, indicating that its propagation direction was affected by the bottom topography. As shown in Fig. 2, two inflection points occurred on February 26, 2017, and March 10, 2017 (indicated by red triangles) and the trajectory shifted toward the southwest and offshore at the two inflection points. From the bathymetry map of the SCS (color shading in Fig. 2), the target eddy moved to deeper regions at both inflection points. Therefore, we suggest that the occurrence of these two inflection points was most likely due to the change of bottom topography, which once again suggests that the movement direction of the eddy was closely related to the bottom topography.

Figure 4 shows the variation of the amplitude, velocity, area-averaged vorticity, or Rossby number ($Ro = \frac{\zeta}{f}$, ζ is area-averaged vorticity, f is the Coriolis parameter). In this way, if the area-averaged vorticity is $-0.3f$, then Ro is -0.3 of the eddy. Before the B-Argo was trapped by the eddy, the eddy was still in a growing stage, the amplitude increased from 7.5 to 14.2 cm, the velocity increased from 35.9 to 56.4 cm s^{-1} , and area-averaged vorticity changed from $-0.16f$ to $-0.28f$. When the B-Argo was trapped by the eddy, the eddy was quite stable, and the dynamic properties reached

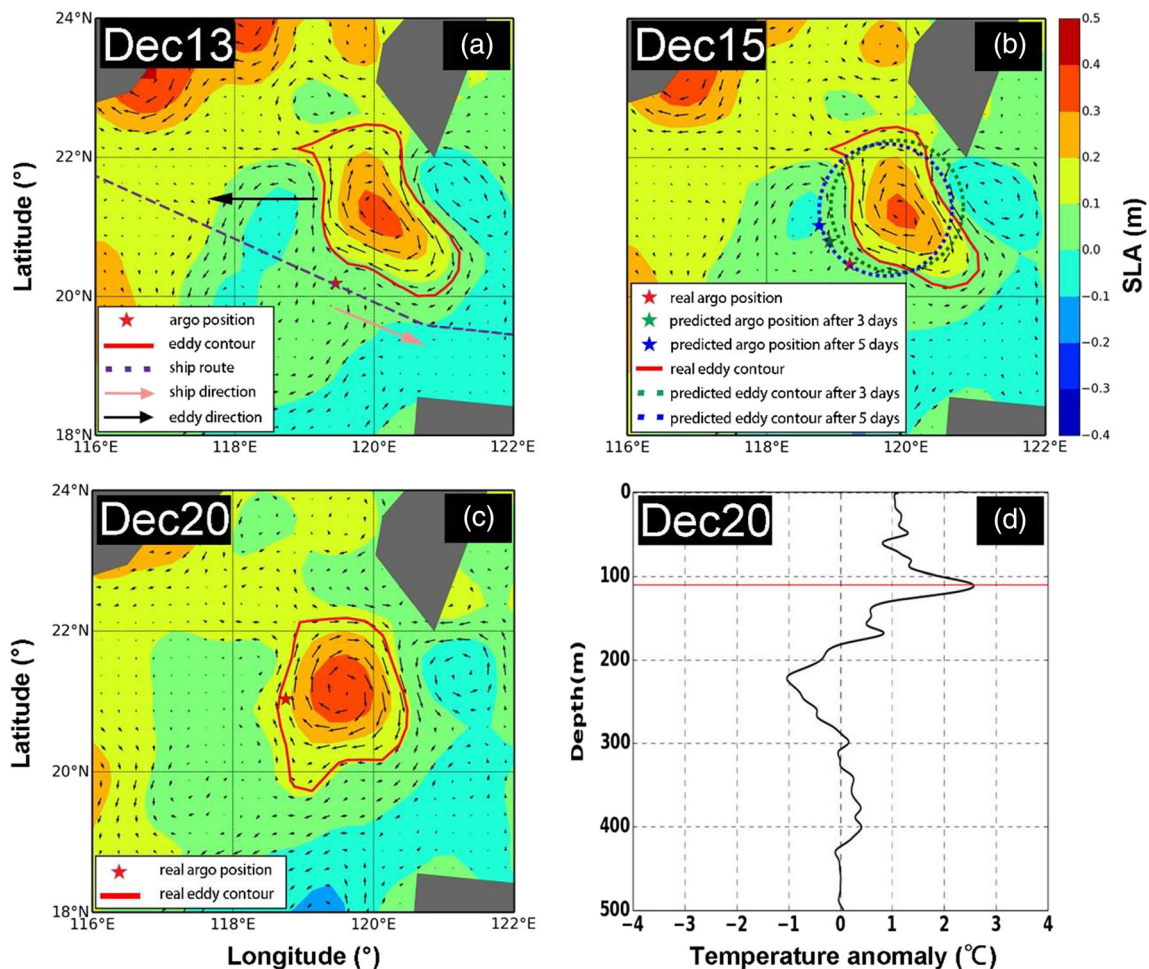


Fig. 3 B-Argo deployment and the target eddy movement prediction. Maps of SLA (m) on December 13 (**a**), 15 (**b**), and 20 (**c**). The eddy boundary is indicated by the red line and the location of the float on each day is indicated by the red star. The purple dashed line in **a** indicates the fixed trajectory of the ship, while the pink and black arrows indicate the direction of ship and eddy respectively. **b** shows the prediction results on December 15. The green dashed line and star

indicate the predicted eddy shape and B-Argo position after 3 days, and the dashed blue line and star denote the predicted state after 5 days. **c** shows the B-Argo and eddy positions on December 20, 2016. **d** shows the temperature anomaly profile from B-Argo on December 20 inferred from the CSIRO climatology. The horizontal red line indicates the location of the maximum TA

their maxima during this period. On January 30, 2017, the amplitude and velocity simultaneously reached 28.63 cm and 73.43 cm s^{-1} , respectively. After January 30, 2017, the surface amplitude, velocity, and area-averaged vorticity began to decline, and this trend continued until the death of the eddy. The eddy parameters changed suddenly on January 14, 2017, when SLA maps show the division of one eddy into two eddies. After the target eddy was splitting into two small eddies (A and B as shown in Fig. 6c and d), we draw continuous amplitude, velocity, and area-averaged vorticity curves using the parameters of small eddy B, whose center was closer to the original eddy center. During the division, the amplitude and velocity dropped suddenly to 1.6 cm and 17.16 cm s^{-1} , respectively, while area-averaged vorticity changed to -0.59 f . In accordance with altimetry, the two eddies merged again on January 18, 2017. We examine this apparent splitting and merger of eddies by using B-Argo data in section 5.2.

5.2 B-Argo movements and target eddy split verification

From December 20, 2016, to February 24, 2017, the B-Argo profiles were collected daily and our experiment finally obtained 62 valid eddy profiles. Trapped by the target eddy, the trajectory of B-Argo was roughly three circles (Fig. 5a–f). At the end of the observation stage, from February 10 to February 24, 2017, the eddy moved quickly and drifted to shallower water. The mission ended on February 24, 2017, when the B-Argo's batteries ran out of energy.

From January 14, 2017, to January 18, 2017, SLA maps highlighted the split of the eddy into two smaller eddies. The position and boundary of these smaller eddies after splitting are plotted in Fig. 6c and d. The distance between the two eddy cores was 28.32 km on January 14, 2017, and 31.86 km on January 18, 2017. After the splitting of the target

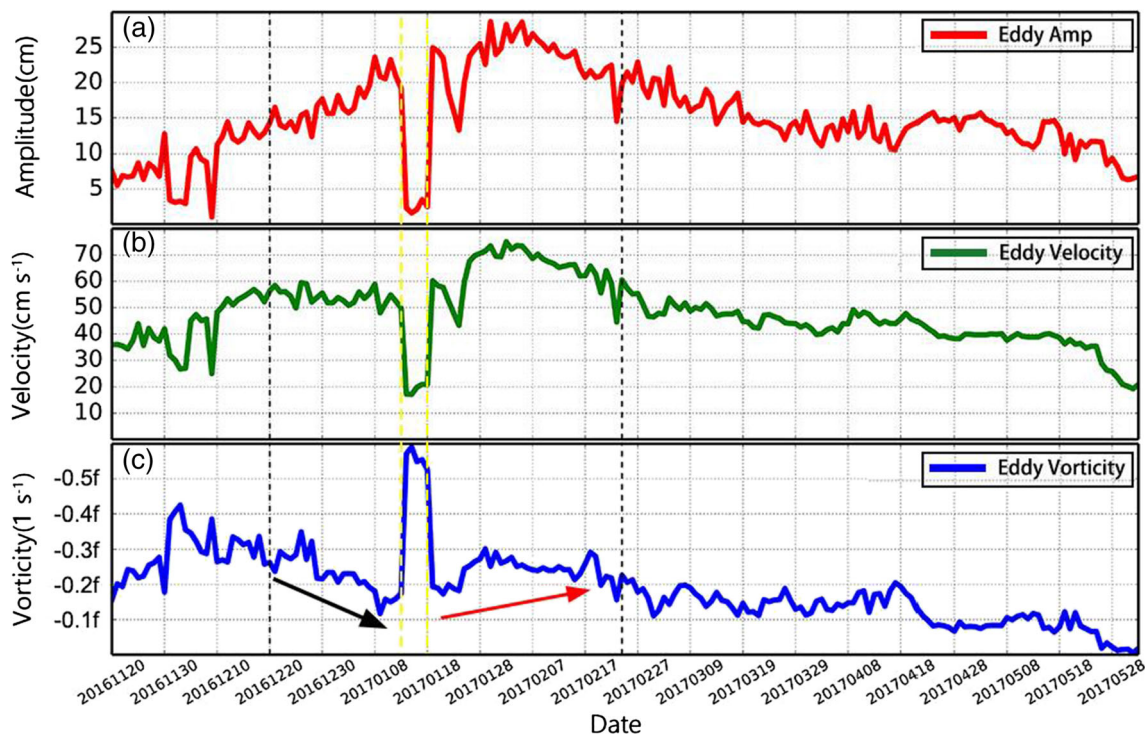


Fig. 4 The amplitude (cm), velocity (cm s^{-1}), area-averaged vorticity (s^{-1}) temporal evolution throughout the eddy life cycle. Black lines indicate the period of B-Argo observations while yellow lines indicate the split and subsequent merger of the eddy seen in SLA data. Blue curve

represents the area-averaged vorticity as a function of Coriolis parameter (f). Black arrow in c represents the downward trend of area-averaged vorticity, while the red arrow represents the rising trend

eddy, the dynamic parameters such as amplitude and maximum geostrophic velocity decreased sharply, while an abrupt increase can be observed in the area-averaged vorticity. However, the heading angle of the B-Argo followed the same regular periodic motion without experiencing sudden changes (Fig. 6b), which suggests that the B-Argo turned around the same eddy. Therefore, the eddy “splitting” observed from altimeter products may be an artifact, which appeared because of the limitation of the radar altimeters detection resolution (Chelton and Schlax 2003). Eddy tracking results obtained from satellite altimeter data may be inaccurate due to their sparse spatiotemporal sampling and instrumental error (Le Traon et al. 1998). This limitation has also been observed by Amores et al. (2018). Thus, continuous profiles of the Argo float can be used to verify and correct the eddy tracking results from altimeter data.

5.3 Temperature/salinity (T/S) profiles obtained by the B-Argo

Eddy temperature and salinity profiles were measured daily by the B-Argo from December 20, 2016, to February 24, 2017. We analyze the temperature and salinity observational data above a depth of 500 m. The thermocline is the transition layer between warmer mixed water at the ocean surface and cooler stratified deeper water, and varies in depth. As shown by the

black line in Fig. 7a, the thermocline depth was generally deeper than 100 m within the eddy. Over the first five profiles, the thermocline was shallower as the B-Argo crossed into the interior of the eddy. While the B-Argo was trapped by the eddy, the thermocline depth was nearly 200 m because the float was closer to the eddy center. Within the continuous spatiotemporal dataset, we can see that there was no fixed value for the depth of the thermocline, but it changed rapidly with different sampling profiles at difference distances from the eddy center. The Argo float 2901480 obtained 10 profiles from March 5, 2017, to April 10, 2017, with a 4-day interval, and the depth of the thermocline varies from ~ 100 to ~ 200 m, similar to the depth range of the thermocline measured by the B-Argo.

Figure 7b shows that the highest salinity in the eddy was 34.9 psu in the subsurface layer at approximately 180 m depth. To better describe the spatiotemporal variability captured by the float, we plotted temperature and salinity anomalies (Fig. 7c and d) by removing the climatological profile referred in section 2.3. The warm anomalies were in the depth range of 100–280 m, while the high-salinity anomalies were from 0 to 50 m depth. The maximum temperature anomaly was 6.4 °C and the maximum salinity anomaly was 0.6 psu. In a study by Chen et al. (2010), the Luzon warm eddy maximum temperature anomaly was 5 °C and the maximum salinity anomaly was 0.5 psu, which appeared at a depth of 100 m. Shu et al.

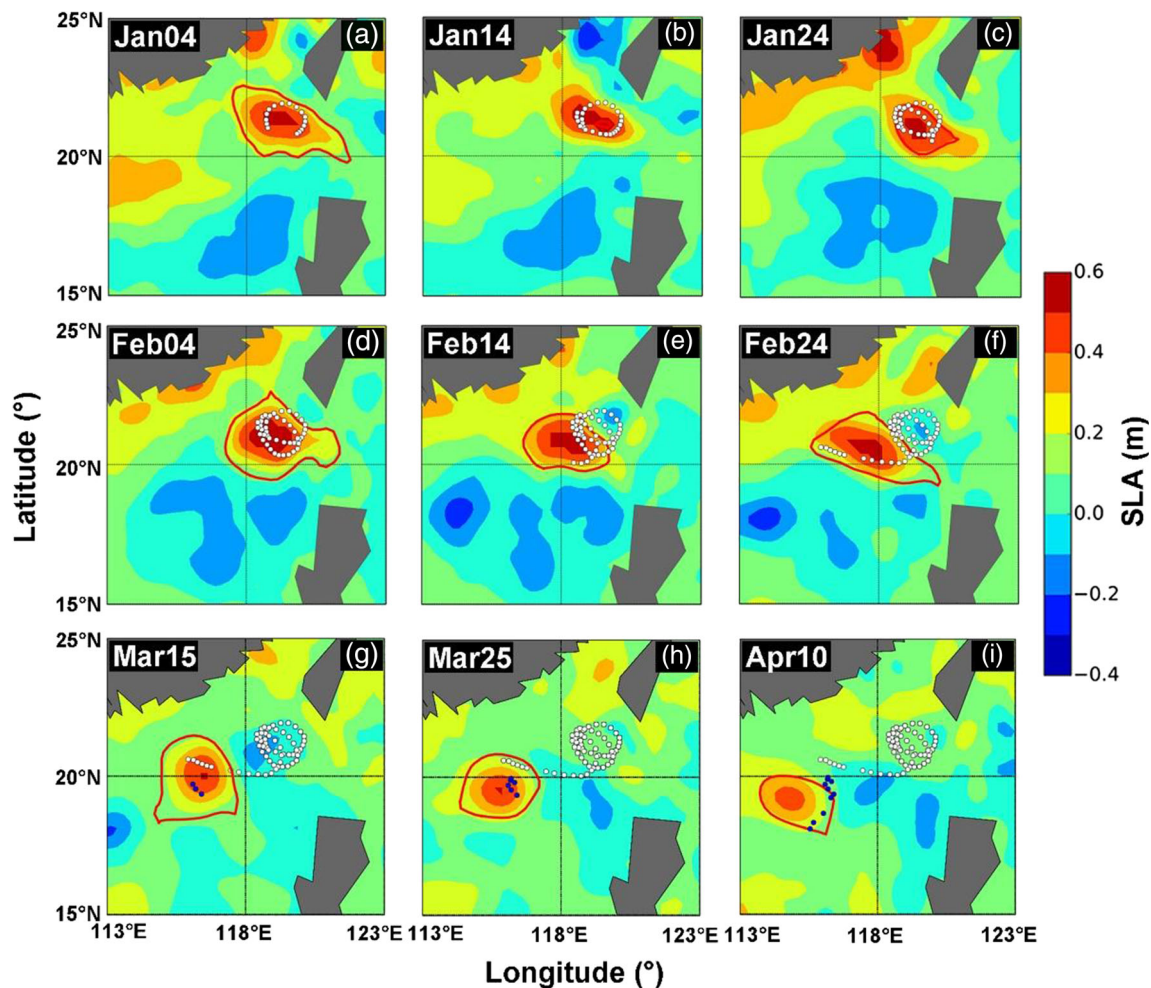


Fig. 5 Argo float trajectory with profile locations (dots), time-varying SLA (color shading), and eddy boundaries (red). White dots in **a–f** indicate the B-Argo profile locations and blue dots in **g–i** show 10 profile locations of the Argo float 2901480

(2016) used a glider to study the small scale structure of an anticyclonic eddy in the northern of SCS. The maximum temperature anomaly was approximately 3 °C, and the maximum salinity anomaly exceeded 0.3 psu, which appeared at 120 m. The generation position and moving directions of the eddy we studied were similar to those of Chen et al. (2010) and Shu et al. (2016), but larger temperature and salinity anomalies were observed.

6 Eddy normalized structure and water source

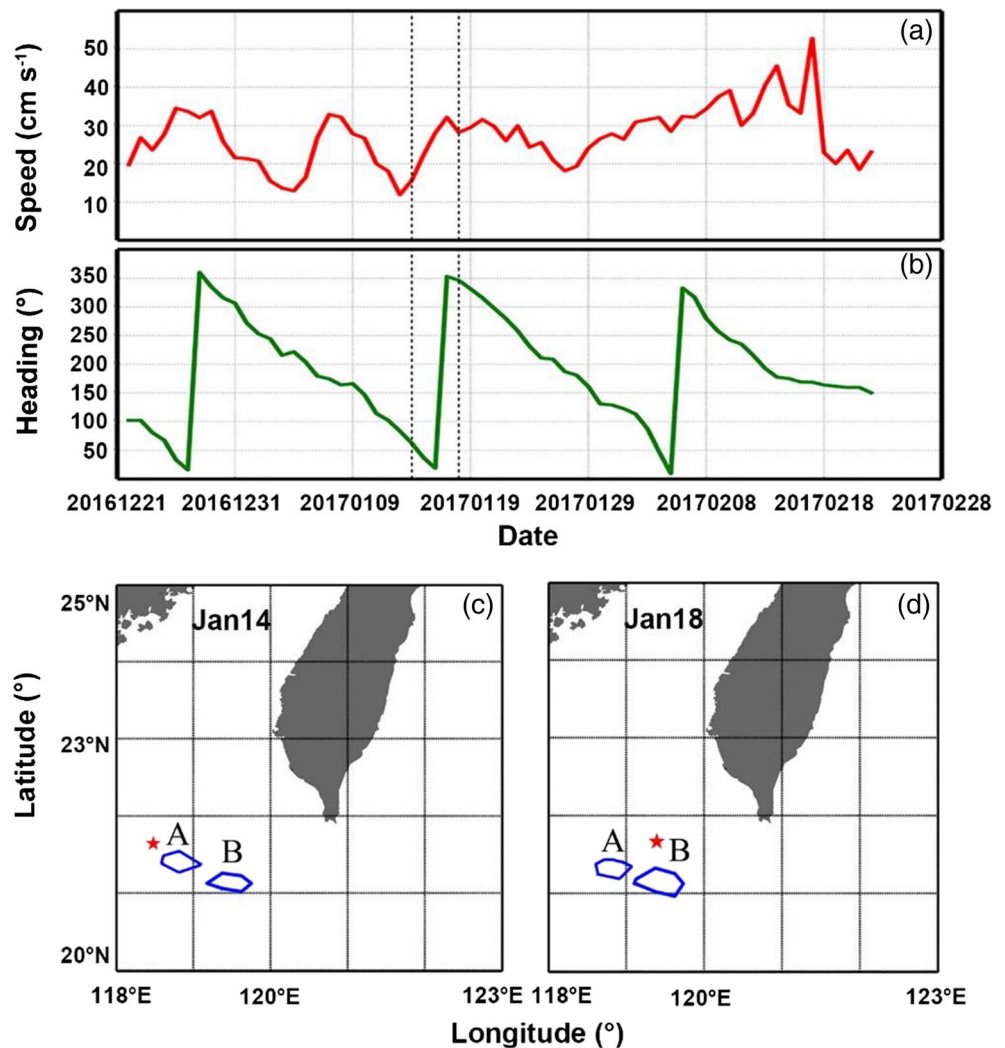
6.1 Radial variability of the anticyclonic eddy

To remove the influence of the eddy radial structure, the normalized radial distance (NRD) of the B-Argo float has been defined as $NRD = r/R$, where r represents the distance from the B-Argo float to the eddy center and R is the radius of the eddy. Figure 8 shows the distribution of NRD in time and space. From December 31, 2016, to February 11, 2017, all

B-Argo profiles were located within the maximum geostrophic velocity boundary (shown by the green stars in Fig. 8), except for anomalies in NRD caused by artifacts observed from satellite altimeters (shown by the red stars in Fig. 8). The reason for these anomalies is that after the original eddy split into two small eddies (small eddy A and B in Fig. 6c and d) from January 14, 2017, to January 18, 2017, the rapid decrease of eddy radius (R) led to the rapid increase of the normalized radial distance ($NRD = r/R$) and several abrupt values. The normalized 2D location of B-Argo profiles relative to eddy center is plotted in Fig. 8b and the radius of three standard circles are $0.5R$, $0.8R$, and R , respectively. Most profiles were distributed between $0.5R$ and $0.8R$ once the float was trapped by the eddy.

The relationship between the NRD of the B-Argo and the area-averaged vorticity or Rossby number of the target anticyclonic eddy could be revealed based on altimeter and the B-Argo data. During the observation period of the B-Argo from December 20, 2016, to January 14, 2017, the area-averaged vorticity and Rossby number of the target eddy show a

Fig. 6 B-Argo parameter changes and eddy “splitting”. Daily B-Argo speed (a) and heading (b) computed from the trajectory. Dashed lines mark the period in which SLA maps indicated the eddy splitting in two and then merged back together. The boundary of the two small eddies and the position of the B-Argo on 14 (c) and 18 (d) January 2017 are indicated by solid blue lines and red stars, respectively



decreasing trend (Fig. 4c), and the NRD has a similar trend as indicated by the black arrow in Fig. 8. The imbalance of radial momentum with decreasing Rossby number drove the B-Argo to be close to the eddy center. Conversely, as indicated by the red arrow in Fig. 4a and 8a, larger Rossby number results in the B-Argo floats being pushed away from the eddy center.

In addition, we study a relation between the depth of the thermocline detected from each profile and NRD of the B-Argo. By comparing the thermocline depth and the NRD (Fig. 8), it is found that the decrease of the NRD corresponds to the increase of the thermocline depth (shown by black arrow); on the contrary, the increase of the NRD corresponds to the decrease of the thermocline depth (shown by red arrow). In other words, the closer the position was to the eddy center, the deeper the thermocline was, which was in accordance with the bowl-like shape of the isotherms in anticyclonic eddies. The same variation characteristics also appear in the profiles obtained by Argo 2901480, where the maximum of the thermocline depth corresponds to the closest position of this float to the eddy center. Both floats show a similar relation between

the depth of the thermocline detected from each profile and the distance of this profile to the eddy center, and this relation could explain the variations in the thermocline depth.

6.2 Eddy water source indicated from B-Argo data

The number of profiles within the effective radius and the speed-based radius are shown in Table 1. An effective radius is defined as the radius of a circle with the same area as the region enclosed by C_{eff} mentioned in section 3.1. Similarly, a speed-based eddy radius is defined as the radius of the circle with the same area as the region enclosed by the counter of SLA with maximum average geostrophic speed, and more detailed explanations can be found in Mason et al. (2014). In Fig. 9, T-S diagram is calculated with the profiles located within the speed-based radius. In addition, two reference T-S curves are plotted by using the average of climatological data (CARS2009) in the red and blue boxes, which represent the regional average characteristics of the SCS water and Kuroshio water respectively.

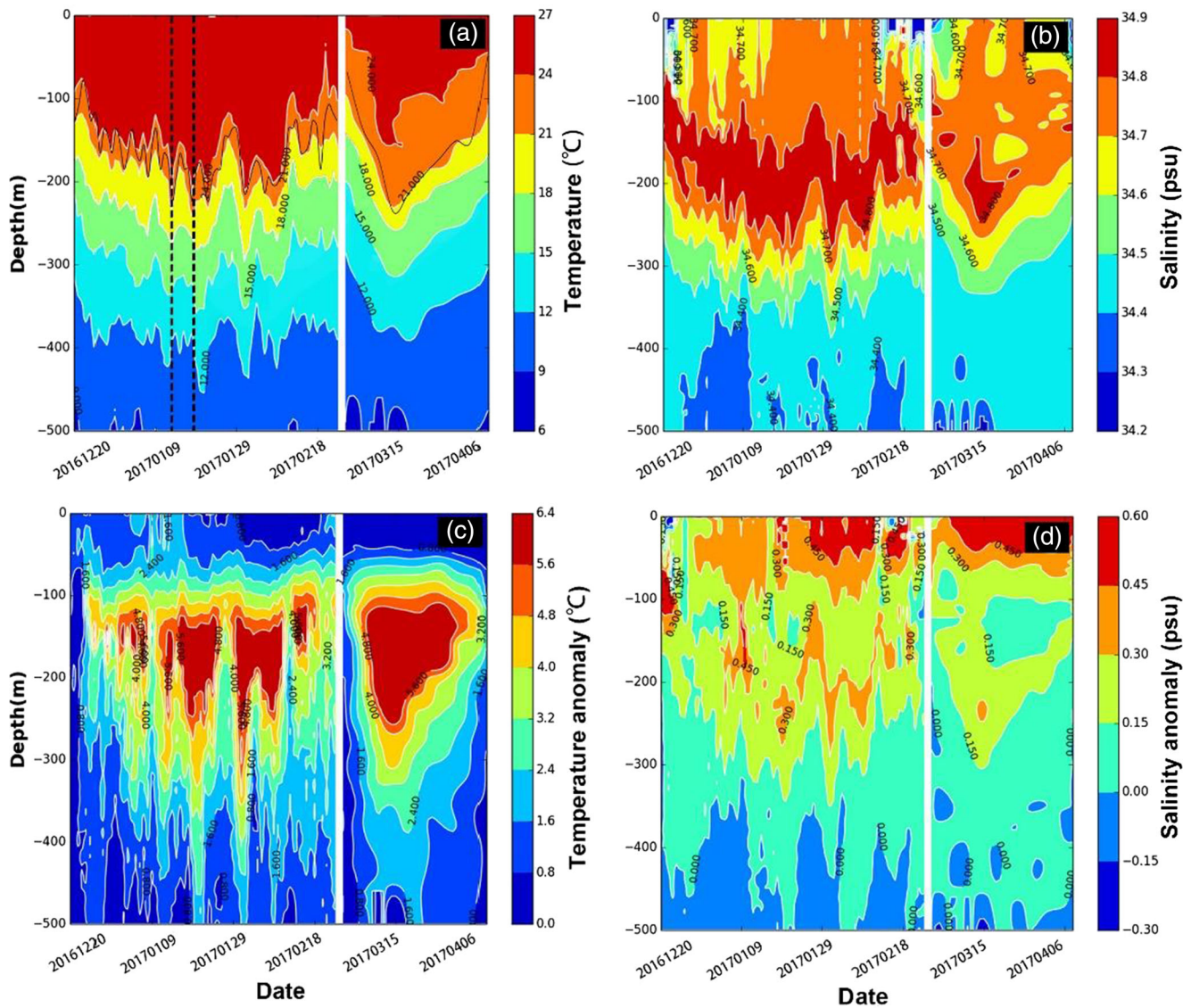


Fig. 7 The daily T/S profiles obtained by the eddy-borne Argo floats. Daily temperature (a) and salinity (b) profiles obtained by the eddy-following Argo floats, and corresponding temperature anomalies (c) and salinity anomalies (d) relative to the CARS2009 climatology. Profiles left of the vertical white line are from the B-Argo, and the

profiles right of the line are from the Argo float 2901480. The black solid line in a represents the upper boundary depth of the thermocline and two vertical black dashed line represents the starting and ending time of eddy splitting

As shown in Fig. 9, we find that the sea water temperature and salinity properties of the B-Argo (green and pink curve) measurements were similar to those of Kuroshio water (blue curve) at the early stage when it was trapped by eddy. At the end of observation of Argo float 2901480 (grass green curve) on April 10, 2017, it is found that temperature and salinity properties in the target eddy began to evolve from the Kuroshio water to the SCS water (purple curve) based on its data.

Two characteristics are revealed from the results. First, the water trapped within the eddy may come from the Kuroshio Current. The earlier T-S curves are close to the Kuroshio water curve while the later T-S curves move closer to the SCS curve.

Second, the T-S diagram from the B-Argo data is very similar to the characteristics of the Kuroshio water but is quite different from those of the surrounding water in the SCS, implying that little exchange occurred between the eddy and surrounding water during the eddy tracking period for the target eddy. According to the analysis from SLA data, the amplitude and area-averaged vorticity of this stage also gradually increased to a stable level, indicating that this anticyclone effectively trapped the Kuroshio water mass and maintained the temperature and salinity characteristics of Kuroshio water in its relatively strong stage.

After the B-Argo was trapped by the target eddy, most of its profiles were located between 0.5R and 0.8R (as shown by

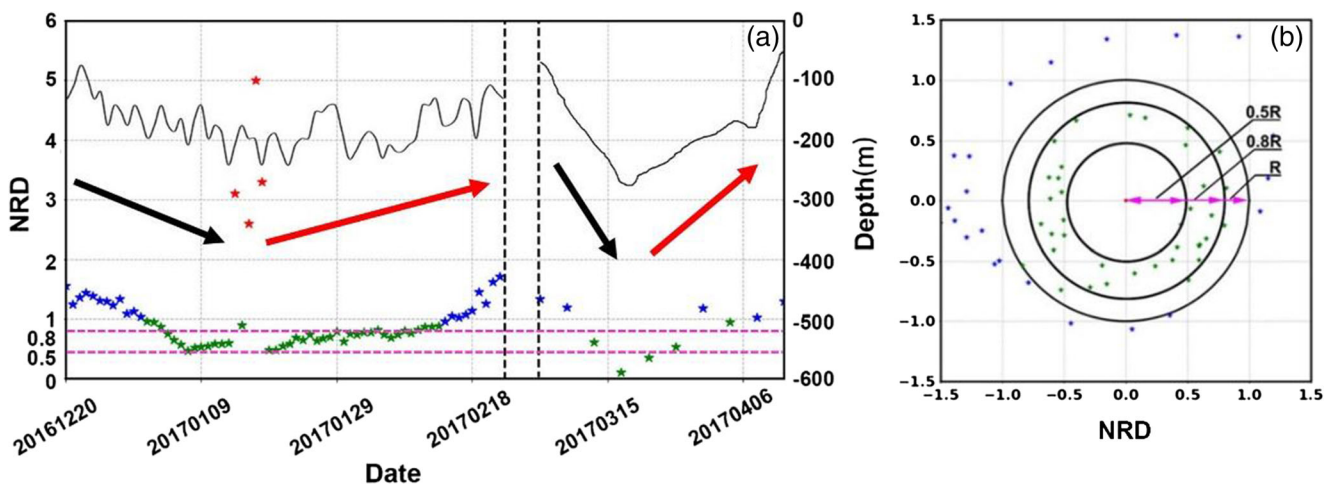


Fig. 8 Normalized radial distance and normalized location. The blue stars plotted in **a** represent the B-Argo with a normalized distance greater than 1.0, the green stars represent a normalized distance less than 1, and the red stars represent anomalies caused by artifacts observed from remote sensing. Black solid line represents the upper boundary depth of the thermocline (also shown in Fig. 7a). Two vertical black dashed line

represents the ending observation time of B-Argo and the starting observation time of Argo 2901480. Black arrow represents the decreasing trend of NRD or thermocline depth, while the red arrow represents the rising trend. **b** shows the normalized position of B-Argo. R is the target eddy radius

green stars in Fig. 8). As shown in Fig. 10, temperature and salinity curves were drawn in different radial ranges with an interval of $0.1R$. There were 9, 8, and 13 profiles participated in drawing the curves of $0.5R-0.6R$ (green), $0.6R-0.7R$ (pink), and $0.7R-0.8R$ (sky blue), respectively. These curves show that profiles at the eddy center have different thermohaline characteristics with profiles at the eddy periphery. At the eddy center, the water can be better isolated from the outside, and have properties similar to those at the Kuroshio, while water at the eddy periphery may be mixed with the water from the surroundings.

7 Summary and concluding remarks

This work proposes a new observational method that used an Argo float to actively track and sample a SCS anticyclonic eddy. Using this method, we successfully conducted an

eddy-borne Argo float measurement experiment in the South China Sea and obtained 62 effective profiles of the target eddy. Temperature and salinity anomalies shown by the profiles indicated that the parameters of the B-Argo were set correctly, especially the parking depth set to 150 m, which is critical. Absence of mutation in heading and velocity of the B-Argo from January 14, 2017, to January 18, 2017, suggested that the eddy splitting process detected from altimeter data should be an artifact.

The subsurface vertical structure of the target eddy was studied using profiles obtained by the B-Argo. Larger temperature anomalies ($6\text{ }^{\circ}\text{C}$) and salinity anomalies (0.6 psu) of the target eddy were greater than that observed by Chen et al. (2010) and Shu et al. (2016). Both the area-averaged vorticity and thermocline depth of the eddy show a relation with the NRD of the float to the eddy center. Among them, the decrease of area-averaged vorticity will drive the B-Argo to move toward the eddy center, while the larger area-averaged

Table 1 Number of profiles within the effective radius and the speed-based radius

Argo float	Time	Total number of profiles	Number of profiles within the effective radius	Number of profiles within the speed-based radius
B-Argo	1–10 days	10	10	0
	11–20 days	9	9	7
	21–30 days	9	5	5
	31–40 days	9	9	9
	41–50 days	10	10	10
	51–60 days	10	10	5
	61–67 days	5	5	0
	Argo 2901480	1–37 days	10	10

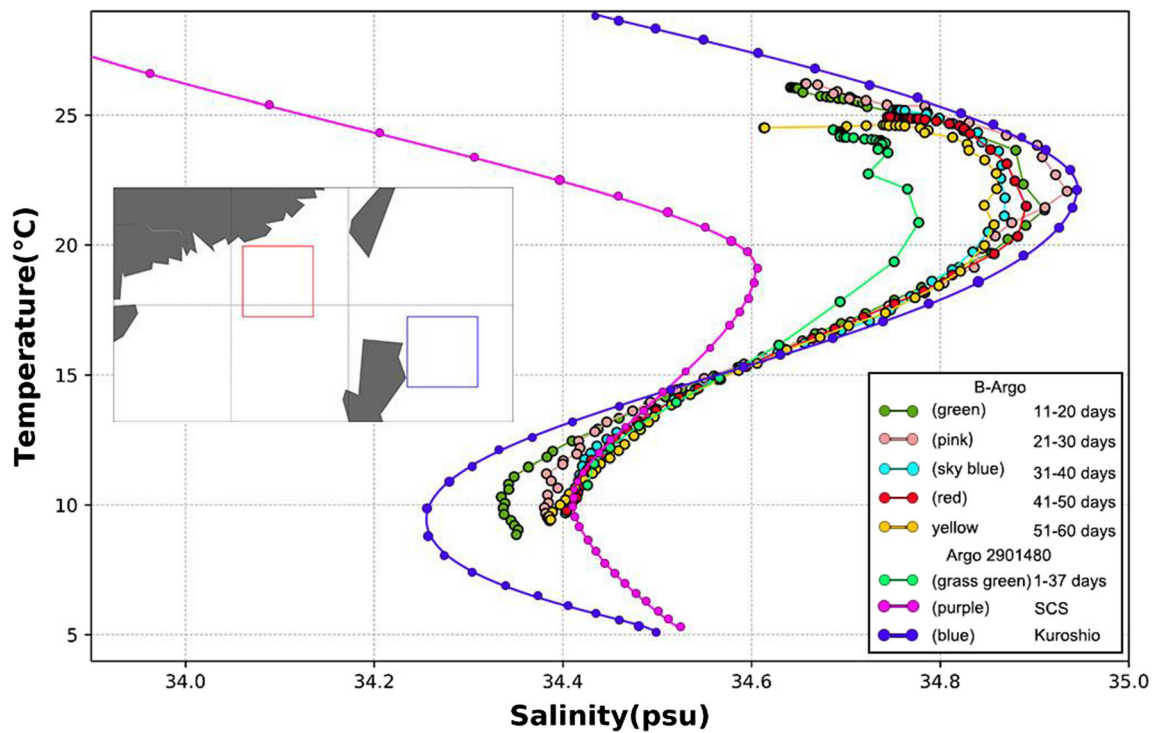


Fig. 9 T-S diagram from Argo profiles. Mean T-S diagram for B-Argo profiles, Argo float 2901480 profiles, SCS water, and Kuroshio water. The SCS and Kuroshio water properties were computed using climatological data within the red and blue boxes, respectively, shown in the insert

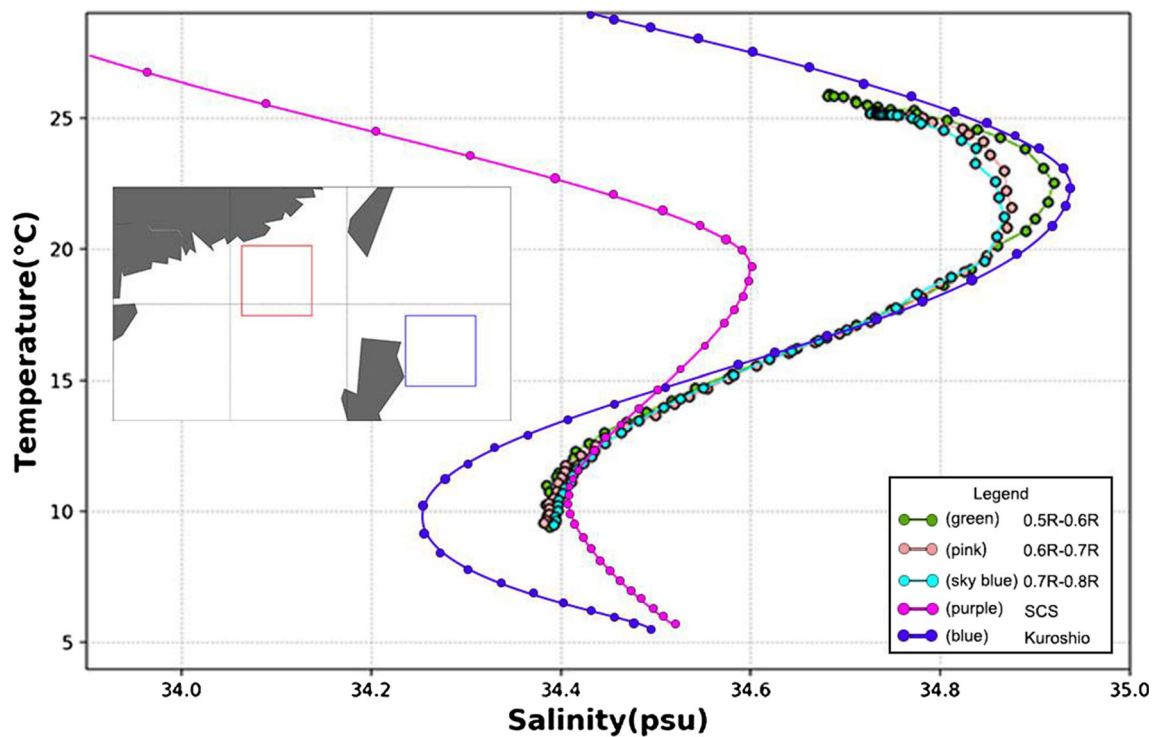


Fig. 10 T-S diagram of the B-Argo profiles with different radial positions. The SCS and Kuroshio water properties were computed using climatological data within the red and blue boxes, respectively, shown in the insert

vorticity results in the B-Argo being pushed away from the eddy center. Through the relationship between the thermocline depth and the NRD of the float, we can infer that the thermocline depth has a bowl-like shape inside the anticyclonic eddies. On the one hand, T-S diagram of 62 profiles obtained by B-Argo from December 20, 2016, to February 24, 2017, is very similar to the characteristics of the Kuroshio water but is quite different from SCS water, indicating the source of eddy water should be from the shedding of the Kuroshio Current. On the other hand, almost no change in thermohaline property also suggested that the eddy water had little exchange with the surrounding water in the SCS.

Compared with mooring, glider, and other observation platforms, an Argo float cost less. Based on the eddy-borne Argo observation method proposed in this work, temperature and salinity profiles that are consecutive in time, homogeneous in space, and similar in NRD can be obtained. These data can be very useful for studying the 3D structure and the evolution of an eddy. It can be predicted that if the observation method is applied to the Argo floats in the global ocean, the amount of effective eddy observation data would greatly increase, which would promote the development of new mesoscale eddy theories. This work is a successful experiment of a new observation strategy to actively track target eddies with Argo floats. In the future, we will track more eddies and obtain more valuable observation data by using the same strategy. For predicting the eddy and B-Argo trajectories, ocean models should be used to improve the prediction accuracies in future work.

Funding information This research was funded by National Natural Science Foundation of China: no. 41906155, the Key Research and Development Program of Shandong Province: no. 2019GHZ023, and the Fundamental Research Funds for the Central Universities: no. 201762005. The National Key Scientific Instrument and Equipment Development Projects of National Natural Science Foundation of China: no. 41527901.

References

- Amores A, Jordà G, Arsouze T, Le Sommer J (2018) Up to what extent can we characterize ocean eddies using present-day gridded altimetric products? *J Geophys Res: Oceans* 123(10):7220–7236. <https://doi.org/10.1029/2018JC014140>
- Chelton DB, Schlax MG (2003) The accuracies of smoothed sea surface height fields constructed from tandem altimeter datasets. *J Atmos Ocean Technol* 20:1276–1302. [https://doi.org/10.1175/1520-0426\(2003\)020<1276:TAOSS>2.0.CO;2](https://doi.org/10.1175/1520-0426(2003)020<1276:TAOSS>2.0.CO;2)
- Chelton DB, Schlax MG, Samelson RM, De Szoeke RA (2007) Global observations of large oceanic eddies. *Geophys Res Lett* 34(15):L15606. <https://doi.org/10.1029/2007GL030812>
- Chelton DB, Schlax MG, Samelson RM (2011) Global observations of nonlinear mesoscale eddies. *Prog Oceanogr* 91(2):167–216. <https://doi.org/10.1016/j.pocean.2011.01.002>
- Chen GX, Hou YJ, Chu XQ, Peng QI (2010) Vertical structure and evolution of the Luzon Warm Eddy. *Chin J Oceanol Limnol* 28(5):955–961. <https://doi.org/10.1007/s00343-010-9040-3>
- Chen GX, Hou YJ, Chu XQ (2011) Mesoscale eddies in the South China Sea: mean properties, spatiotemporal variability, and impact on thermohaline structure. *J Geophys Res Oceans* 116(C6):C06018. <https://doi.org/10.1029/2010JC006716>
- Chen GX, Gan JP, Xie Q, Chu XQ, Wang DX, Hou YJ (2012) Eddy heat and salt transports in the South China Sea and their seasonal modulations. *J Geophys Res* 117(C5):C05021. <https://doi.org/10.1029/2011JC007724>
- Chen GX, Wang DX, Dong CM, Zu TT, Xue HJ, Shu YQ (2015) Observed deep energetic eddies by seamount wake. *Sci Rep* 5(17):416. <https://doi.org/10.1038/srep17416>
- Chu XQ, Xue HJ, Qi YQ, Chen GX, Mao QW, Wang DX, Chai F (2014) An exceptional anticyclonic eddy in the South China Sea in 2010. *J Geophys Res* 119(2):881–897. <https://doi.org/10.1002/2013JC009314>
- Dong CM, McWilliams JC, Liu Y, Chen D (2014) Global heat and salt transports by eddy movement. *Nat Commun* 5:3294. <https://doi.org/10.1038/ncomms4294>
- Dufau C, Orszynowicz M, Dibarboure G, Morrow R, Le Traon P-Y (2016) Mesoscale resolution capability of altimetry: present and future. *J Geophys Res: Oceans* 121(7):4910–4927. <https://doi.org/10.1002/2015JC010904>
- Ester M, Kriegel H-P, Sander J, Xu XW (1996) A density-based algorithm for discovering clusters a density-based algorithm for discovering clusters in large spatial databases with noise. *Int Conf Knowl Discov Data Min* 96:226–331
- He QY, Zhan HG, Cai SQ, He YH, Huang GL, Zhan WK (2018) A new assessment of mesoscale eddies in the South China Sea: surface features, three-dimensional structures and thermohaline transports. *J Geophys Res: Oceans* 123(7):4906–4929. <https://doi.org/10.1029/2018JC014054>
- Hu JY, Zheng QA, Sun ZY, Tai CK (2011) Study of a mesoscale anticyclonic eddy in the western part of the Gulf of Lion. *J Mar Syst* 88(1):3–11. <https://doi.org/10.1016/j.jmarsys.2011.02.008>
- Hu JY, Zheng QN, Sun ZY, Tai C-K (2012) Penetration of nonlinear Rossby eddies into South China Sea evidenced by cruise data. *J Geophys Res* 117(C3):C03010, 339. <https://doi.org/10.1029/2011JC007525>
- Le Traon PY, Nadal F, Ducet N (1998) An improved mapping method of multisatellite altimeter data. *J Atmos Ocean Technol* 15(2):522–534. [https://doi.org/10.1175/1520-0426\(1998\)015<0522:AIMMOM>2.0.CO;2](https://doi.org/10.1175/1520-0426(1998)015<0522:AIMMOM>2.0.CO;2)
- Lee JG, Han JW, Whan KY (2007) Trajectory clustering: a partition-and-group framework. *Proceedings of the 2007 ACM SIGMOD international conference on Management of data, ACM*, pp. 593–604. <https://doi.org/10.1145/1247480.1247546>
- Li C, Zhang ZW, Tian JW, Zhao W (2017) A statistical study on the subthermocline submesoscale eddies in the northwestern Pacific Ocean based on Argo data. *J Geophys Res: Oceans* 122(5):3586–3598. <https://doi.org/10.1002/2016JC012561>
- Liu YJ, Chen G, Sun M, Liu S, Tian FL (2016) A parallel sla-based algorithm for global mesoscale eddy identification. *J Atmos Ocean Technol* 33(12):2743–2754. <https://doi.org/10.1175/JTECH-D-16-0033.1>
- Mason E, Pascual A, McWilliams JC (2014) A new sea surface height-based code for oceanic mesoscale eddy tracking. *J Atmos Ocean Technol* 31:1181–1188. <https://doi.org/10.1175/JTECH-D-14-00019.1>
- Nan F, He ZG, Zhou H, Wang DX (2011) Three long-lived anticyclonic eddies in the northern South China Sea. *J Geophys Res* 116(C5):C05002. <https://doi.org/10.1029/2010JC006790>

- Nan F, Xue HJ, Yu F (2015) Kuroshio intrusion into the South China Sea: a review. *Prog Oceanogr* 137:314–333. <https://doi.org/10.1016/j.pocean.2014.05.012>
- Penven P, Echevin V, Pasapera J, Colas F, Tam J (2005) Average circulation, seasonal cycle, and mesoscale dynamics of the Peru current system: a modeling approach. *J Geophys Res: Oceans* 110(C10):C10021. <https://doi.org/10.1029/2005JC002945>
- Shu YQ, Xiu P, Xue HJ, Yao JL, Yu JC (2016) Glider-observed anticyclonic eddy in northern South China Sea. *Aquat Ecosyst Health Manag* 19(3):233–241. <https://doi.org/10.1080/14634988.2016.1208028>
- Shu YQ, Chen J, Li S, Wang Q, Yu JC, Wang DX (2018) Field-observation for an anticyclonic mesoscale eddy consisted of twelve gliders and sixty-two expendable probes in the northern South China Sea during summer 2017. *Sci China Earth Sci* 62(2):451–458. <https://doi.org/10.1007/s11430-018-9239-0>
- Sun M, Tian FL, Liu YJ, Chen G (2017) An improved automatic algorithm for global eddy tracking using satellite altimeter data. *Remote Sens* 3(3):206. <https://doi.org/10.3390/rs9030206>
- Tian FL, Wu D, Yuan LM, Chen G (2020) Impacts of the efficiencies of identification and tracking algorithms on the statistical properties of global mesoscale eddies using merged altimeter data. *Int J Remote Sens* 41(8):2835–2860. <https://doi.org/10.1080/01431161.2019.1694724>
- Wade IP, Heywood KJ (2001) Tracking the PRIME eddy using satellite altimetry. *Deep-Sea Res II Top Stud Oceanogr* 48(4):725–737. [https://doi.org/10.1016/S0967-0645\(00\)00094-1](https://doi.org/10.1016/S0967-0645(00)00094-1)
- Wang GH, Su JL, Chu P (2003) Mesoscale eddies in the South China Sea observed with altimeter data. *Geophys Res Lett* 30(2121):2121. <https://doi.org/10.1029/2003GL018532>
- Wang Q, Zeng LL, Zhou WD, Xie Q, Cai SQ, Wang DX (2015) Mesoscale eddies cases study at Xisha waters in the South China Sea in 2009/2010. *J Geophys Res: Oceans* 120(1):517–532. <https://doi.org/10.1002/2014JC009814>
- Xiu P, Chai F, Shi L, Xue H, Chao Y (2010) A census of eddy activities in the South China Sea during 1993–2007. *J Geophys Res: Oceans* 115(C3):C03012. <https://doi.org/10.1029/2009JC005657>
- Xu LX, Li PL, Xie SP, Liu QY, Liu C, Gao WD (2016) Observing mesoscale eddy effects on mode-water subduction and transport in the North Pacific. *Nat Commun* 7(10):505. <https://doi.org/10.1038/ncomms10505>
- Yuan DL, Han WQ, Hu DX (2007) Anti-cyclonic eddies northwest of Luzon in summerfall observed by satellite altimeters. *Geophys Res Lett* 34(13):L13610. <https://doi.org/10.1029/2007GL029401>
- Zaba KD, Rudnick DL (2016) The 2014–2015 warming anomaly in the southern California Current System observed by underwater gliders. *Geophys Res Lett* 43(3):1241–1248. <https://doi.org/10.1002/2015GL067550>
- Zhang ZW, Zhao W, Tian JW, Liang XF (2013) A mesoscale eddy pair southwest of Taiwan and its influence on deep circulation. *J Geophys Res: Oceans* 118(12):6479–6494. <https://doi.org/10.1002/2013JC008994>
- Zhang ZG, Wang W, Qiu B (2014) Oceanic mass transport by mesoscale eddies. *Science* 345(6194):322–324. <https://doi.org/10.1126/science.1252418>
- Zhang WZ, Xue HJ, Chai F, Ni QB (2015) Dynamical processes within an anticyclonic eddy revealed from Argo floats. *Geophys Res Lett* 42(7):2342–2350. <https://doi.org/10.1002/2015GL063120>
- Zhang ZW, Tian JW, Qiu B, Zhao W, Chang P, Wu DX, Wan XQ (2016) Observed 3d structure, generation, and dissipation of oceanic mesoscale eddies in the South China Sea. *Sci Rep* 6(24):349. <https://doi.org/10.1038/srep24349>
- Zhong YS, Bracco AL, Tian JW, Dong JH, Zhao W, Zhang ZW (2017) Observed and simulated submesoscale vertical pump of an anticyclonic eddy in the South China Sea. *Sci Rep* 7:44011. <https://doi.org/10.1038/srep44011>